



# Ultrasonography-assisted near-infrared spectroscopy imaging enhanced by gold nanorods in a xenograft mouse model of prostate cancer

Seungsoo Lee<sup>1</sup>, Dae Chul Jung<sup>2</sup>, Seung-seob Kim<sup>2</sup>, Jaemoon Yang<sup>2</sup>, Yoochan Hong<sup>3</sup>, Dalkwon Koh<sup>4</sup>

<sup>1</sup>Department of Radiology, Yongin Severance Hospital, Research Institute of Radiological Science, Yonsei University College of Medicine, Yongin; <sup>2</sup>Department of Radiology, Severance Hospital, Research Institute of Radiological Science, Yonsei University College of Medicine, Seoul; <sup>3</sup>Department of Medical Devices, Korea Institute of Machinery and Materials, Daejeon; <sup>4</sup>Department of Biomicrosystem Engineering, Korea University College of Health Science, Seoul, Korea

**Purpose:** This study aimed to develop and evaluate a near-infrared spectroscopy (NIRS) system enhanced by gold nanorods (GNRs) for the detection of prostate cancer using phantom and xenograft mouse models.

**Methods:** A hybrid ultrasound-NIRS (US-NIRS) system was created with a 785 nm wavelength, integrating eight laser diodes and four detectors with a linear ultrasound probe. Software for processing near-infrared (NIR) signals was developed using an engineering toolkit and an image reconstruction package. Two optical phantoms simulating prostate cancer were constructed using TiO<sub>2</sub> for scattering effects and India ink for absorption effects, each containing a cylindrical cavity for GNRs positioned at depths of 1 cm and 2 cm. A xenograft mouse model was prepared by injecting PC-3 cells into the right flank of nude mice. PEGylated GNRs (GNR-PEG) were synthesized. US-NIRS imaging was performed on mice before and after intravenous injection of GNR-PEG.

**Results:** Ultrasonography revealed solid, vascular tumors without necrosis or hemorrhage. Pre-injection NIRS showed higher baseline NIR absorbance in tumors compared to normal tissue (optical depths: 0.26, 1.52, and 0.24 for the 1.5 cm, 1.4 cm, and 0.5 cm tumors, respectively). After GNR-PEG injection, tumor optical depths significantly increased (3.36, 4.39, and 1.69 for the 1.5 cm, 1.4 cm, and 0.5 cm tumors, respectively), peaking around 5 minutes, and subsequently decreasing towards baseline levels by 60 minutes.

**Conclusion:** A US-NIRS hybrid imaging system enhanced by GNR-PEG demonstrated increased NIR absorption in prostate cancer xenografts. This fusion imaging technique holds potential for future clinical applications in detecting prostate cancer.

**Keywords:** Prostatic neoplasms; Near-infrared spectroscopy; Ultrasonography; Gold; Xenograft

**Key points:** A hybrid ultrasound–near-infrared spectroscopy (US-NIRS) system using PEGylated gold nanorods (GNR-PEG) as a contrast agent was developed to increase near-infrared (NIR) absorbance, improving prostate cancer detection by highlighting tumor neovascularization. Phantom and xenograft mouse model tests confirmed that the US-NIRS system with GNR-PEG significantly enhances tumor NIR absorbance, suggesting clinical applicability for prostate cancer detection.

## ULTRASONOGRAPHY

### ORIGINAL ARTICLE

<https://doi.org/10.14366/usg.25072>  
eISSN: 2288-5943  
Ultrasonography 2025;44:363-371

Received: April 27, 2025

Revised: June 26, 2025

Accepted: July 8, 2025

#### Correspondence to:

Dae Chul Jung, MD, PhD, Department of Radiology, Severance Hospital, Research Institute of Radiological Science, Yonsei University College of Medicine, 50-1 Yonsei-ro, Seodaemun-gu, Seoul 03722, Korea

Tel. +82-2-2228-7400

Fax. +82-2-393-3035

E-mail: DAECHUL@yuhs.ac

This is an Open Access article distributed under the terms of the Creative Commons Attribution Non-Commercial License (<http://creativecommons.org/licenses/by-nc/4.0/>) which permits unrestricted non-commercial use, distribution, and reproduction in any medium, provided the original work is properly cited.

Copyright © 2025 Korean Society of Ultrasound in Medicine (KSUM)



#### How to cite this article:

Lee S, Jung DC, Kim SS, Yang J, Hong Y, Koh D. Ultrasonography-assisted near-infrared spectroscopy imaging enhanced by gold nanorods in a xenograft mouse model of prostate cancer. *Ultrasonography*. 2025 Sep;44(5):363-371.

## Introduction

The incidence of prostate cancer has steadily increased since 1975, largely due to screening for asymptomatic disease using the prostate-specific antigen test. However, a concurrent decline in mortality rates has raised concerns regarding overtreatment risks and complications from invasive diagnostic methods [1,2]. Clinically significant prostate cancer is characterized by a Gleason score of 7 or higher (including grade group 3+4), a tumor volume of at least 0.5 cm<sup>3</sup>, or extraprostatic extension [3,4]. Consequently, active surveillance has emerged as a viable management strategy for patients with low-risk disease, offering an alternative to immediate curative treatment [5,6].

However, a key challenge in active surveillance is the limited sensitivity of transrectal ultrasound (TRUS) for cancer detection. Thus, TRUS-guided systematic random biopsy carries a considerable risk of missing or understaging clinically significant lesions [7,8]. Notably, approximately 25% of cases initially diagnosed on biopsy are upgraded to a higher Gleason score following pathological examination of the entire radical prostatectomy specimen [9,10].

To address these limitations, noninvasive optical techniques such as near-infrared spectroscopy (NIRS) have emerged as promising diagnostic tools. NIRS employs light in the 700–900 nm range. Here, light scattering dominates over absorption, enabling deep tissue penetration to facilitate the measurement of concentrations and distributions of endogenous chromophores. Because prostate cancer exhibits higher microvascular density compared to normal prostate tissue, diagnostic feasibility has already been demonstrated in preclinical phantom and animal studies using multichannel NIRS systems [11–15].

Furthermore, employing gold nanorods (GNRs), which absorb light around 800 nm, as contrast agents may further amplify the near-infrared (NIR) absorption signal associated with tumor neovascularity. In the present study, the authors aimed to develop and evaluate a ultrasound-NIRS (US-NIRS) system enhanced by PEGylated GNRs (GNR-PEG) using an optical phantom and a prostate cancer xenograft mouse model.

## Materials and Methods

### Compliance with Ethical Standards

The study was conducted with the approval of the Institutional Animal Care and Use Committee of the authors' institution and conformed to the guidelines of the National Institutes of Health for the care and use of laboratory animals.

### Multi-channel US-NIRS Imaging System

The NIRS system employed a continuous-wave method for NIR signal measurement. Eight laser diodes (Thorlabs, Newton, NJ, USA) operating at wavelengths of 785 nm and 830 nm were used as NIR sources, alongside four avalanche photodiodes (APDs; Hamamatsu Photonics, Hamamatsu City, Japan) serving as detectors. Optical fibers with a diameter of 400 μm (FT400-EMT, Thorlabs) were connected to the laser diodes and APDs. To mitigate interference from ambient light, the setup incorporated bandpass filters, root mean square detectors, and low-pass filters for 6 kHz and 25 kHz frequency modulation of light. A microcontroller unit (ATmega128, Atmel, San Jose, CA, USA) collected and transmitted data via serial communication to a personal computer. A graphical user interface for processing incoming signals and displaying relative NIR absorption on a logarithmic scale was designed using LabVIEW (National Instruments, Austin, TX, USA) and NIRFAST (Dartmouth College and University of Birmingham) software packages [16]. Integration of the ultrasound device (Aixplorer, SuperSonic Imagine, Aix-en-Provence, France) probe with the NIRS system facilitated imaging. In the combined NIRS system, the light emitters were evenly spaced 0.3 cm apart and attached to the linear ultrasound probe (Fig. 1). The signal receivers were anchored on the opposite side of the ultrasound probe, 2 cm from the emitters.

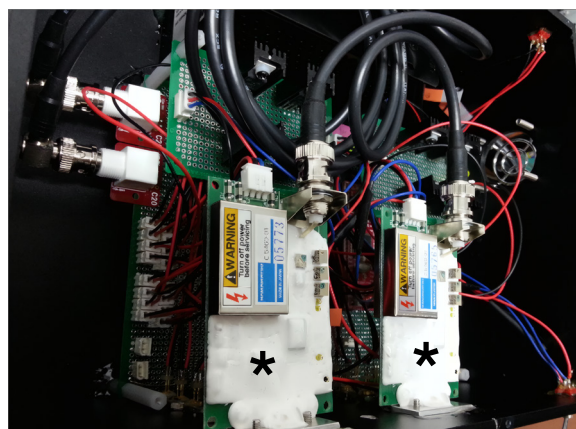
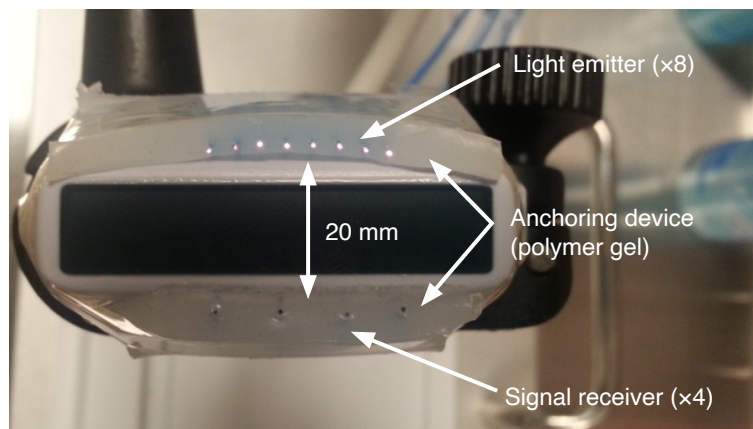
### Synthesis of GNR-PEG

GNRs were synthesized using a seed-mediated growth method. A gold seed solution was prepared by combining 0.25 mL of 10 mM HAuCl<sub>4</sub> solution with 7.5 mL of 93 mM aqueous cetyltrimethylammonium bromide (CTAB) solution. Sodium borohydride (0.6 mL, 10 mM) was added as a reducing agent. This process yielded individual gold seed nanoparticles coated with CTAB molecules (CTA-AuBr<sub>4</sub>). Subsequently, a growth solution was prepared by mixing 0.08 mL of 10 mM silver nitrate solution, 0.05 mL of 10 mM HAuCl<sub>4</sub> solution, and 9.5 mL of 95 mM CTAB solution, with 55 μL of 100 mM ascorbic acid added as a reducing agent. When the color of the growth solution changed from yellow to colorless, 12 μL of the gold seed solution was introduced, stirred for 10 seconds, and incubated for 24 hours. During incubation, the solution changed from colorless to reddish-brown. Excess CTAB molecules were removed from the GNR solution by centrifugation at 15,000 rpm for 30 minutes, and the product was dispersed in 5 mL of deionized water. For PEGylation of the CTAB-coated GNRs (4.73 mM), 50 mg of mPEG-SH (Mw 5K) was added; this was followed by mixing for 24 hours at room temperature, then centrifuging again at 15,000 rpm for 30 minutes to remove unbound PEG molecules. The resulting product was suspended in 5 mL of deionized water.

The morphology of GNR-PEG was examined using transmission

electron microscopy (Fig. 2). The aspect ratio (longitudinal to transverse length) was approximately 3.6. The absorption spectrum

of the GNR-PEG solution displayed a maximum absorption peak at 780 nm in the NIR region.



**A**  
**Fig. 1.** Ultrasound–near-infrared spectroscopy imaging system.

**A.** The integrated probe comprises eight optical fibers linked to laser diodes (light emitters) and four optical fibers for detectors, positioned on the opposite side of the ultrasound probe. **B.** Internal components of the near-infrared spectroscopy system are illustrated. Optical fibers are affixed to two avalanche photodiodes (asterisks), which serve as detectors to convert near-infrared signals into electrical signals.

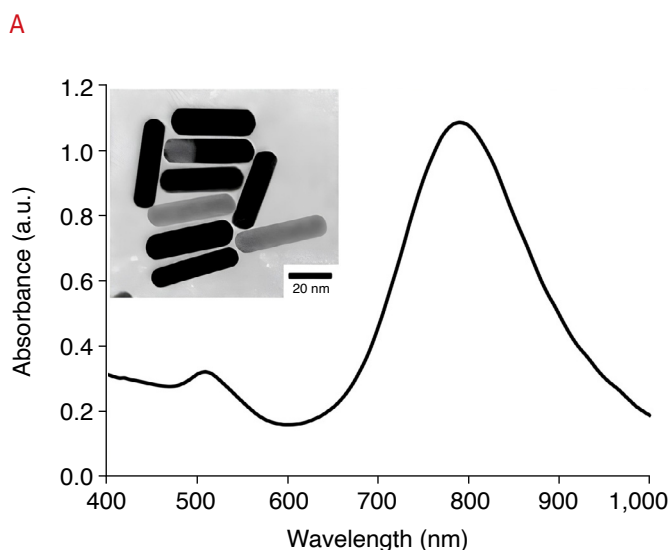
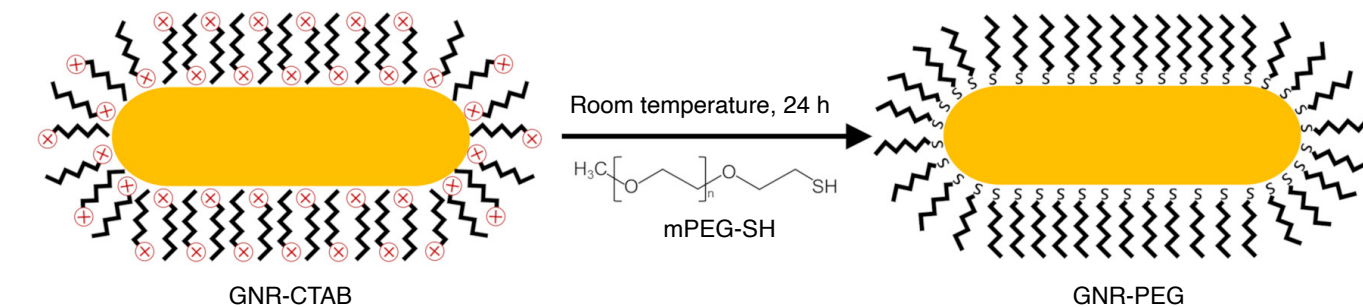


**Fig. 2.** Schematic illustration of PEGylated gold nanorods (GNR-PEG).

**A.** PEGylation of cetyltrimethylammonium bromide–coated GNRs (GNR-CTAB) was performed by adding mPEG-SH (Mw 5K) and mixing for 24 hours at room temperature. **B.** Transmission electron microscopic image and absorption spectrum of GNR-PEG solution are presented.

**B**

### Optical Phantom of Prostate Cancer

To replicate the optical characteristics of a prostate gland, an optical phantom was created using TiO<sub>2</sub> to simulate scattering effects and India ink to simulate absorption effects. The optical properties of typical prostate tissue were calibrated using reference values from prior studies, and adjustments were made by incorporating precise amounts of TiO<sub>2</sub> and India ink into the phantom (volume, 200 mL; TiO<sub>2</sub>, 0.252 g; India ink, 0.064 g;  $\mu_s'$  10/cm, 785 nm;  $\mu_a$  0.2/cm, 785 nm) [17–20]. Cylindrical empty spaces to be filled with GNRs were prepared with depths of 1 cm and 2 cm and a diameter of 1 cm.

### Xenograft Model of Prostate Cancer

BALB/c nude mice (Orient Bio Inc., Seongnam, Korea) aged 4–6 weeks were anesthetized with a Zoletil/Rompun mixture administered via intraperitoneal injection. PC-3 prostate cancer cell lines were procured from the Korean Cell Line Bank and cultured in RPMI 1640 medium (Gibco, Invitrogen, Carlsbad, CA, USA) supplemented with 10% fetal bovine serum and 1% antibiotics. The incubator was maintained at 37°C with a humidified atmosphere of 5% CO<sub>2</sub>. Subcutaneous injections of  $5 \times 10^6$  human prostate cancer cells were administered into the mouse flank. *In vivo* imaging using ultrasonography and NIRS was conducted when the tumors reached a diameter of approximately 1.0 cm. All experiments were performed with the approval of the Association for Assessment and Accreditation of Laboratory Animal Care.

### Ultrasonography and NIRS of Optical Phantom and Xenograft Mouse with GNR-PEG

The change in optical depth ( $\Delta OD$ ) resulting from the absorption of the material can be calculated using the formula:  $\Delta OD = \ln(I_c/I_e)$ , where  $I_c$  represents the intensity of the light detected during the calibration phase and  $I_e$  denotes the intensity of the light detected during the enhanced phase with the absorption material, such as GNR-PEG. Ultrasonography and NIRS were performed on an optical phantom containing GNR-PEG at four different concentrations (15  $\mu$ g, 5  $\mu$ g, 1.5  $\mu$ g, and 0.5  $\mu$ g of Au in 1 mL of solution) at depths of 1 cm and 2 cm (Fig. 3). For *in vivo* imaging of mouse tumors, ultrasonography and NIRS were conducted under anesthesia. GNR-PEG (15  $\mu$ g Au in 100  $\mu$ L solution) were administered via tail-vein injection, and ultrasonography and NIRS imaging were repeated after 5, 40, and 60 minutes (Fig. 4).

## Results

### *In Vitro* NIRS Imaging of the Phantom with Four Different GNR-PEG Concentrations

The maximal optical depths measured at a depth of 1 cm were 0.64,

1.70, 1.43, and 1.57 at concentrations of 0.5, 1.5, 5.0, and 15  $\mu$ g/mL, respectively. At a depth of 2 cm, the optical depths at the same concentrations were 0.51, 1.31, 1.51, and 1.21 (Fig. 5).

### *In Vivo* US-NIRS Imaging of the Xenograft Mice with PC-3 Tumors

Ultrasound imaging of the mice revealed tumors in the subcutaneous layer (Fig. 6). The tumor diameters were approximately 1.5 cm, 1.4 cm, and 0.5 cm, with depths less than 0.2 cm. The tumors exhibited internal vascularity and homogeneous echotexture without signs of necrosis or hemorrhagic degeneration. These ultrasound characteristics remained consistent after the injection of GNR-PEG.

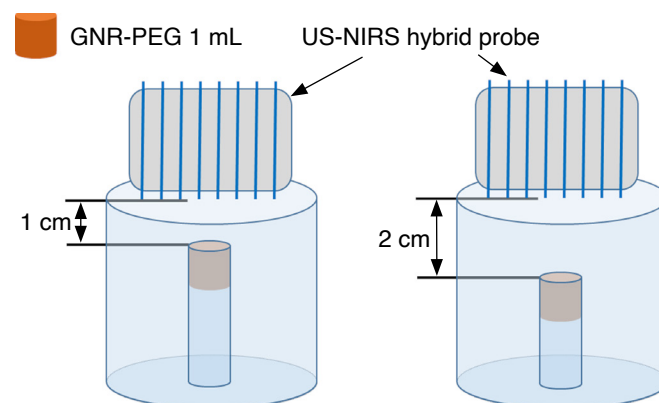


**Fig. 3.** Schematic illustration of the optical phantoms. Ultrasound–near-infrared spectroscopy (US-NIRS) of the optical phantoms was conducted using PEGylated gold nanorods (GNR-PEG) simulating prostate cancer at depths of 1 cm and 2 cm.



**Fig. 4.** Ultrasound–near-infrared spectroscopy (US-NIRS) of the xenograft mice. US-NIRS was performed on the PC-3 tumor (arrowhead) and the opposite flank of xenograft mice, before and after injection of PEGylated gold nanorods.

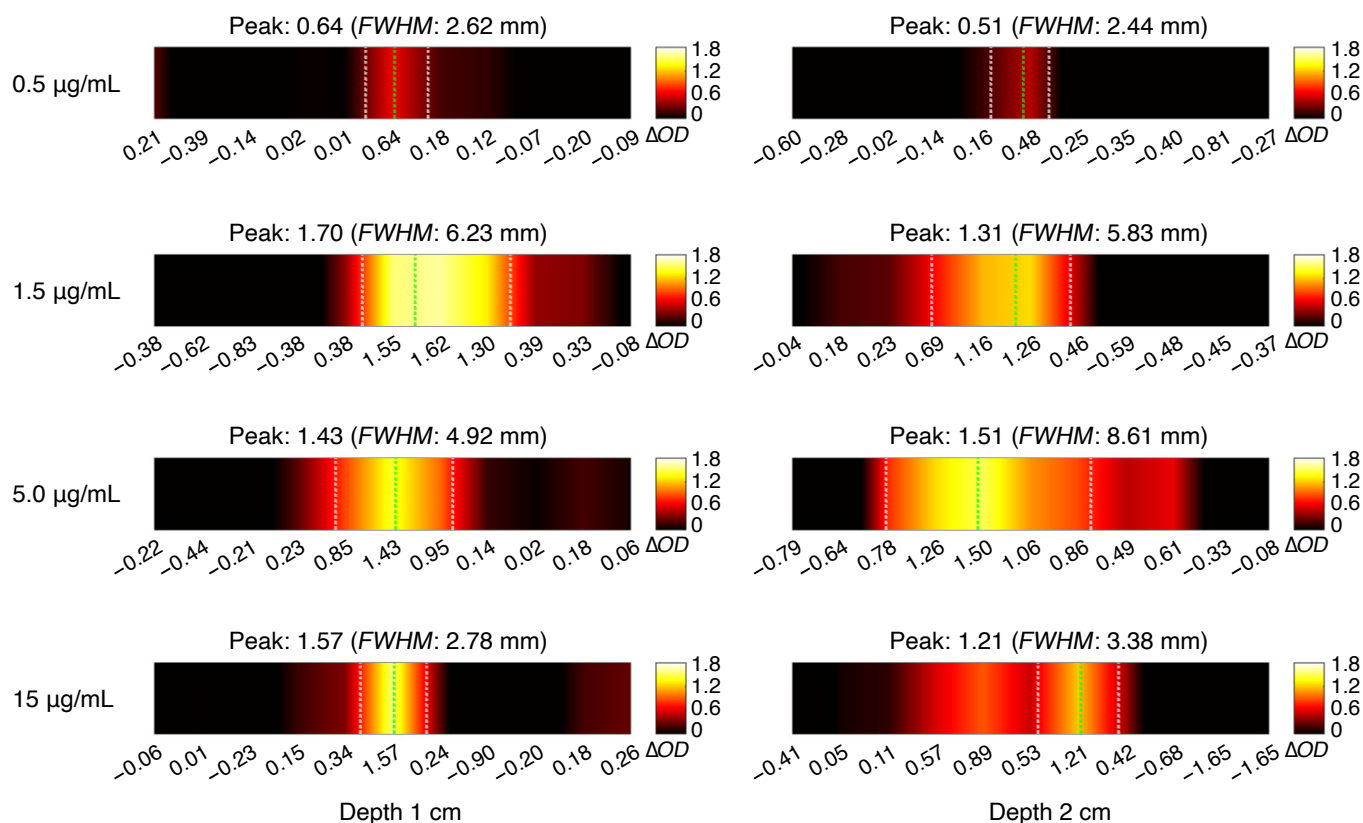


**Fig. 5.** Near-infrared spectroscopy results of the optical phantom at four concentrations. Peak changes in optical depth ( $\Delta OD$ ) and full width at half-maximum (FWHM) are provided. The x-axis spans 2.2 cm. Absorbance increased with rising concentrations of gold nanorods and was more pronounced at a depth of 1 cm compared to 2 cm.

Before GNR-PEG injection, NIRS imaging of the tumors was performed. The optical depths of the tumors (1.5 cm, 1.4 cm, and 0.5 cm) were higher—0.30, 1.57, and 0.30, respectively—compared to the opposite side without a tumor.

Five minutes after GNR-PEG injection, repeated NIRS imaging revealed optical depths of 3.36, 4.40, and 2.12 for the respective tumors. At 40 minutes, the optical depth had decreased to 2.15, 3.90, and 1.87, respectively, and at 60 minutes post-injection, it had further decreased to 0.40, 1.88, and 0.30.

## Discussion

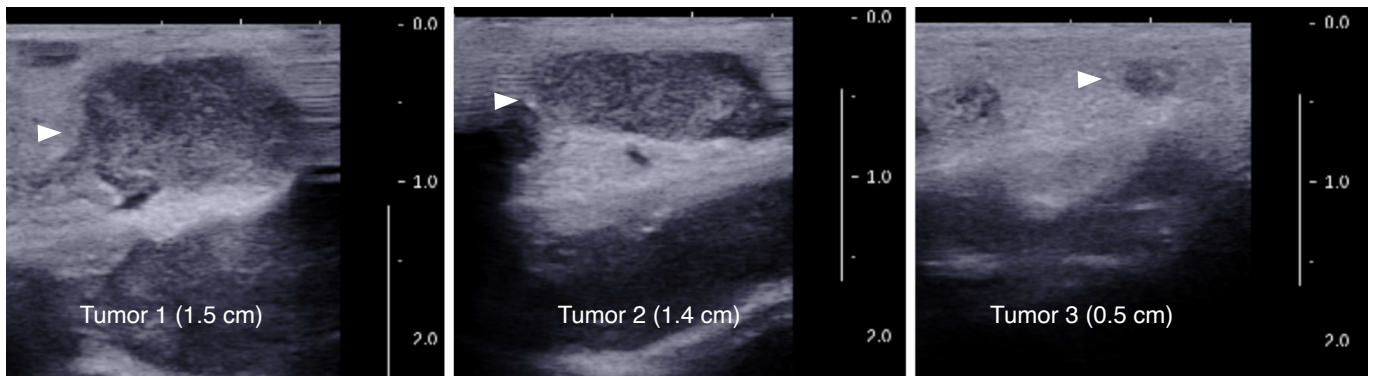
In a previous study, a hybrid US-NIRS imaging system was developed, enabling simultaneous noninvasive acquisition of anatomical and optical data. In the present research, phantom and xenograft models of prostate cancer demonstrated the effectiveness of GNR-PEG in enhancing tumor absorbance using this hybrid imaging system.

NIR light at wavelengths of 785 and 830 nm can effectively penetrate deep into human tissue, enabling quantification of

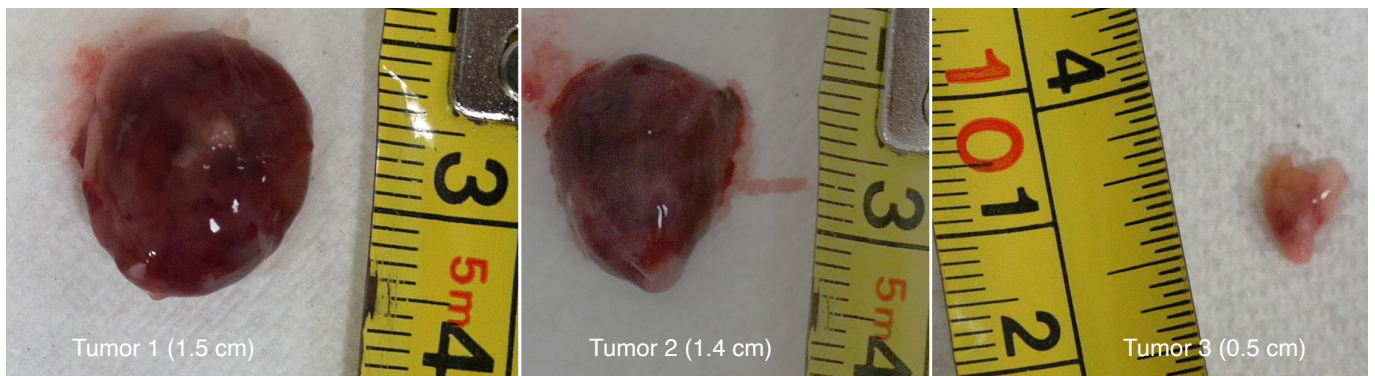
chromophore concentrations in tumors with increased vascularity or accumulated hemoglobin content. Prior investigations employing NIRS for canine transmissible venereal tumors demonstrated detectable NIR absorption linked to heightened vascularity and hemoglobin content, even without enhancing materials [14,15]. However, absorbance alone may be insufficient for detecting small or low-grade cancers. Additionally, anterior prostate cancers should often be assessed using a transperineal approach, necessitating the detection of cancers situated at a greater distance.

In the phantom study, absorbance increased with higher concentrations of GNRs and was more pronounced at a depth of 1 cm compared to 2 cm. However, the absorbance increase did not exhibit a directly proportional relationship with increasing concentration and decreasing distance, indicating potential efficacy of GNRs even under less favorable conditions.

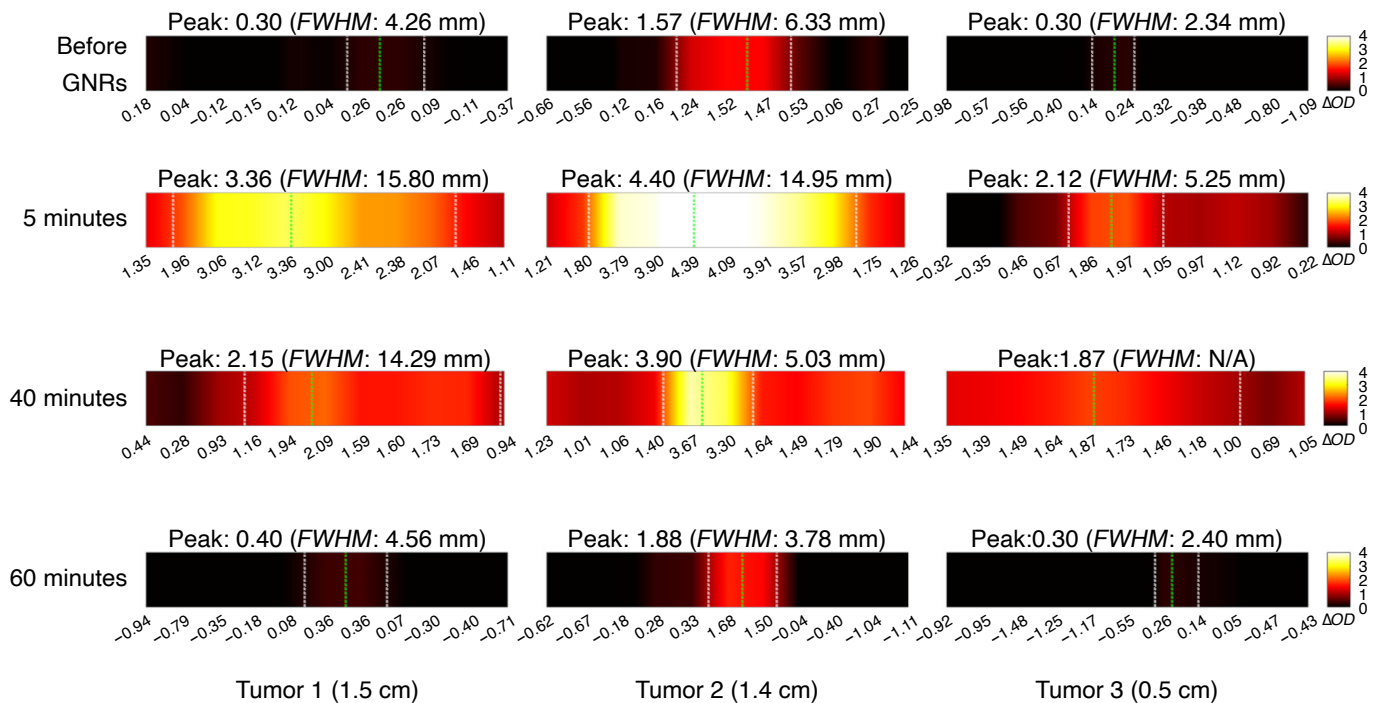
Ultrasonography in this study did not reveal tumor necrosis or hemorrhage, which could have caused unexpected or exaggerated NIR absorption. Thus, optical contrast prior to GNR-PEG administration was solely influenced by the intrinsic vascularity of the tumor. After the GNR-PEG were administered, the optical



A



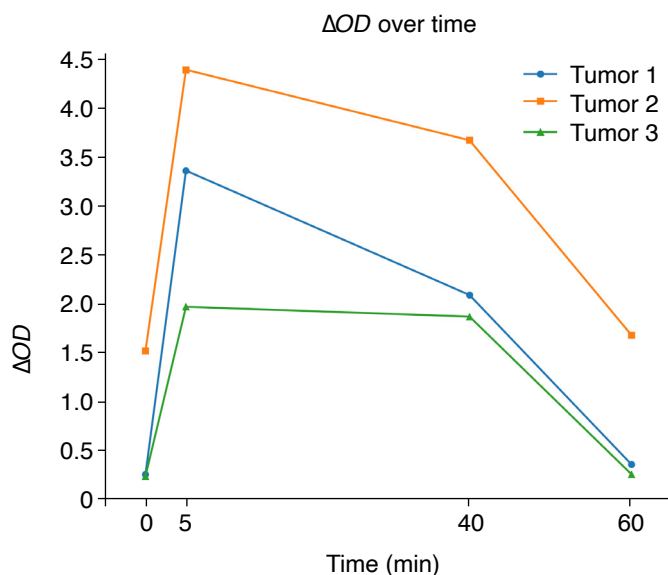
B



C

**Fig. 6.** *In vivo* ultrasound–near-infrared spectroscopy (US-NIRS) of xenograft mouse.

A. The US image of the tumors (arrowheads) reveals no hemorrhagic or necrotic components. B. Photographs of PC-3 tumor specimens are shown. C. *In vivo* NIRS results are presented, including peak optical depth changes ( $\Delta OD$ ) and full width at half-maximum. The x-axis spans 2.2 cm. Tumors were detectable on NIRS even without PEGylated gold nanorods (GNR-PEG). FWHM, full width at half-maximum; N/A, not available.



D

**Fig. 6. D.** The OD of the tumors increased further following administration of GNR-PEG, peaked at 5 minutes post-administration, and returned to pre-administration values at 60 minutes.

depth of the tumors increased further until peaking at 5 minutes post-administration. This phenomenon can be attributed to tumor-bound GNRs. PEGylation is known to increase half-life by evading the reticuloendothelial system and increases concentration by promoting accumulation within tumor cells. A similar effect presumably occurred in this study. The subsequent decrease in optical depth at 40 and 60 minutes is likely due to clearance by the reticuloendothelial system.

The xenograft model exhibited a more pronounced increase in optical depth compared to the phantom. Regarding concentration, if all the administered GNRs were collected in the tumor, the intratumoral GNR concentration would be the same or lower than the phantom's concentration (15  $\mu\text{g}$ , 5  $\mu\text{g}$ , 1.5  $\mu\text{g}$ , and 0.5  $\mu\text{g}$  of Au in 1 mL), thus yielding a maximum concentration of 15  $\mu\text{g}$ . The higher optical depth in the xenograft model could be attributed to the absence of alternative pathways for NIR absorption. The tumor depth (0.2 cm) was shallower than the phantom depths (1 and 2 cm). Additionally, the tumor diameter was larger in the horizontal plane compared to the area of GNRs in the phantom; thus, a larger and nearer tumor could block the NIR course at a wider angle, increasing optical depth. A similar absorption level observed in the smallest tumor (0.5 cm diameter) and the phantom is explained by this same reasoning.

Since minimizing overdiagnosis and overtreatment is essential in modern prostate cancer care, the development goals for US-

NIRS should align accordingly. Prostate cancer tissues with high Gleason scores are expected to exhibit more pronounced enhanced permeability effects. Unlike dynamic contrast-enhanced magnetic resonance imaging (MRI), in which high-grade prostate cancer shows high  $k_{ep}$  values with low-molecular-weight gadolinium agents, macromolecular agents such as GNR-PEG or albumin-bound indocyanine green are expected to exhibit low  $k_{ep}$  values [21]. The potential advantage of NIRS lies in detecting the resulting high retention within prostate tissues. Conversely, benign lesions or low-risk cancers with minimal enhanced permeability and retention effects would produce significantly weaker NIR absorption [22]. Further research is necessary to confirm this signal difference and to identify the optimal imaging time point to maximize contrast, enabling comparative analyses with dynamic contrast-enhanced MRI.

This experiment had several limitations. Initially, phantoms were assessed using GNRs at depths of 1 cm and 2 cm; however, a similar assessment of tumors at varying depths was not performed. This limitation arose because positioning deep-seated tumors within xenograft mouse models is not feasible, potentially necessitating the use of larger animal models such as rats or canines. Furthermore, a key consideration is the ability to investigate tumors at more distant locations. This is particularly relevant for prostate cancer because, although most cases are found in the posterior region of the prostate, a substantial number develop in the anterior portion, distant from the rectal border. For example, transition zone cancers, often enlarged by benign prostatic hyperplasia, can be situated considerably far from the posterior surface. Therefore, evaluating the efficacy of this GNR-enhanced NIR absorption method for detecting these distant tumors is necessary and may require reconfiguring the placement of the emitters and detectors.

Second, in this study, a linear-shaped ultrasound probe was used, unlike the convex probe typically employed for TRUS. The differing arrangements of emitters and receivers necessary for a convex probe with a shorter width could influence the efficacy of NIRS. Although a linear probe is available for TRUS, its arrangement differs markedly from the probe used in this study. Third, a form of sensitivity bias exists wherein higher absorption is detected when a tumor is closer to the detector than the emitter, due to a wider blocking angle. To overcome this limitation, two-dimensional (2D) NIRS reconstruction is required. A feasible solution is to implement a circular array of NIR sources and detectors encompassing the periphery of the US probe. This arrangement is generally considered ideal for 2D tomography, and given the cylindrical shape of a TRUS probe, its application in future studies is highly promising. A fourth limitation involves potential signal interference. Structures with very high OD, as well as common prostatic conditions such as calcification and

inflammation, can adversely affect spatial resolution and signal-to-noise ratio, potentially masking tumor signals. Consequently, the capability of the NIRS system to spatially resolve multiple distinct structures warrants further investigation. Fifth, the current clinical use of GNRs in humans is limited. Indocyanine green, which shares NIR absorption properties with GNRs, is more biocompatible and is already used in clinical practice, making it a potential alternative agent. Lastly, because PEGylation is not an active targeting method for prostate cancer, various complicating factors might exist in individual patients. The recent use of small molecule ligands that bind to the extracellular portion of the prostate-specific membrane antigen, such as PSMA-11, holds promise for the delivery of GNRs or other NIR absorbents [23].

A US-NIRS hybrid imaging system enhanced by GNR-PEG demonstrated increased NIR absorption in tumors in a xenograft mouse model of prostate cancer. This fusion imaging technique shows potential for future clinical applications in the detection of prostate cancer.

ORCID: Seungsoo Lee: <https://orcid.org/0000-0002-6268-575X>; Dae Chul Jung: <https://orcid.org/0000-0001-5769-5083>; Seung-seob Kim: <https://orcid.org/0000-0001-6071-306X>; Jaemoon Yang: <https://orcid.org/0000-0001-7365-0395>; Yoochan Hong: <https://orcid.org/0000-0002-6345-9877>; Dalkwon Koh: <https://orcid.org/0009-0006-1894-4378>

### Author Contribution

Conceptualization: Lee S, Jung DC, Yang J. Data acquisition: Lee S, Jung DC, Kim SS, Yang J, Hong Y. Data analysis or interpretation: Lee S, Jung DC, Hong Y, Koh D. Drafting of the manuscript: Lee S. Critical revision of the manuscript: Lee S, Jung DC, Kim SS, Yang J, Hong Y, Koh D. Approval of the final version of the manuscript: all authors.

### Conflict of Interest

Dae Chul Jung serves as Editor for the *Ultrasonography*, but has no role in the decision to publish this article. All remaining authors have declared no conflicts of interest.

### Acknowledgments

This work was supported by the National Research Foundation of Korea (NRF) grant funded by the Korea government (MSIT) (RS-2025-00558877).

## References

1. Siegel RL, Miller KD, Wagle NS, Jemal A. Cancer statistics, 2023. *CA Cancer J Clin* 2023;73:17-48.
2. Lee MS, Moon MH, Kim CK, Park SY, Choi MH, Jung SI, et al. Guidelines for transrectal ultrasonography-guided prostate biopsy: Korean Society of Urogenital Radiology consensus statement for patient preparation, standard technique, and biopsy-related pain management. *Korean J Radiol* 2020;21:422-430.
3. Epstein JI, Walsh PC, Carmichael M, Brendler CB. Pathologic and clinical findings to predict tumor extent of nonpalpable (stage T1c) prostate cancer. *JAMA* 1994;271:368-374.
4. Turkbey B, Rosenkrantz AB, Haider MA, Padhani AR, Villeirs G, Macura KJ, et al. Prostate Imaging Reporting and Data System version 2.1: 2019 update of Prostate Imaging Reporting and Data System version 2. *Eur Urol* 2019;76:340-351.
5. Hugosson J, Carlsson S, Aus G, Bergdahl S, Khatami A, Lodding P, et al. Mortality results from the Goteborg randomised population-based prostate-cancer screening trial. *Lancet Oncol* 2010;11:725-732.
6. Lee CH, Tan TW, Tan CH. Multiparametric MRI in active surveillance of prostate cancer: an overview and a practical approach. *Korean J Radiol* 2021;22:1087-1099.
7. Ahmed HU, El-Shater Bosaily A, Brown LC, Gabe R, Kaplan R, Parmar MK, et al. Diagnostic accuracy of multi-parametric MRI and TRUS biopsy in prostate cancer (PROMIS): a paired validating confirmatory study. *Lancet* 2017;389:815-822.
8. Park JJ, Kim CK. Paradigm shift in prostate cancer diagnosis: pre-biopsy prostate magnetic resonance imaging and targeted biopsy. *Korean J Radiol* 2022;23:625-637.
9. Epstein JI, Feng Z, Trock BJ, Pierorazio PM. Upgrading and downgrading of prostate cancer from biopsy to radical prostatectomy: incidence and predictive factors using the modified Gleason grading system and factoring in tertiary grades. *Eur Urol* 2012;61:1019-1024.
10. Guichard G, Larre S, Gallina A, Lazar A, Faucon H, Chemama S, et al. Extended 21-sample needle biopsy protocol for diagnosis of prostate cancer in 1000 consecutive patients. *Eur Urol* 2007;52:430-435.
11. Bae H, Kim SS, Lee S, Song H, Lee S, Koh D, et al. Development of a multi-channel NIRS-USG hybrid imaging system for detecting prostate cancer and improving the accuracy of imaging-based diagnosis: a phantom study. *Ultrasonography* 2019;38:143-148.
12. Kragh M, Quistorff B, Lund EL, Kristjansen PE. Quantitative estimates of vascularity in solid tumors by non-invasive near-infrared spectroscopy. *Neoplasia* 2001;3:324-330.
13. Feng Y, Jeong EK, Mohs AM, Emerson L, Lu ZR. Characterization of tumor angiogenesis with dynamic contrast-enhanced MRI and biodegradable macromolecular contrast agents in mice. *Magn Reson Med* 2008;60:1347-1352.
14. Jiang Z, Holyoak GR, Bartels KE, Ritchey JW, Xu G, Bunting CF, et al. In vivo trans-rectal ultrasound-coupled optical tomography of a transmissible venereal tumor model in the canine pelvic canal. *J Biomed Opt* 2009;14:030506.

15. Jiang Z, Piao D, Holyoak GR, Ritchey JW, Bartels KE, Slobodov G, et al. Trans-rectal ultrasound-coupled spectral optical tomography of total hemoglobin concentration enhances assessment of the laterality and progression of a transmissible venereal tumor in canine prostate. *Urology* 2011;77:237-242.
16. Dehghani H, Eames ME, Yalavarthy PK, Davis SC, Srinivasan S, Carpenter CM, et al. Near infrared optical tomography using NIRFAST: algorithm for numerical model and image reconstruction. *Commun Numer Methods Eng* 2008;25:711-732.
17. Simpson CR, Kohl M, Essenpreis M, Cope M. Near-infrared optical properties of ex vivo human skin and subcutaneous tissues measured using the Monte Carlo inversion technique. *Phys Med Biol* 1998;43:2465-2478.
18. Svensson T, Andersson-Engels S, Einarsdottir M, Svanberg K. In vivo optical characterization of human prostate tissue using near-infrared time-resolved spectroscopy. *J Biomed Opt* 2007;12:014022.
19. Zhu TC, Dimofte A, Finlay JC, Stripp D, Busch T, Miles J, et al. Optical properties of human prostate at 732 nm measured in mediated photodynamic therapy. *Photochem Photobiol* 2005;81:96-105.
20. Sandell JL, Zhu TC. A review of in-vivo optical properties of human tissues and its impact on PDT. *J Biophotonics* 2011;4:773-787.
21. Choi MH, Lee YJ, Han D, Kim DH. Quantitative analysis of prostate MRI: correlation between contrast-enhanced magnetic resonance fingerprinting and dynamic contrast-enhanced MRI parameters. *Curr Oncol* 2023;30:10299-10310.
22. Nichols JW, Bae YH. EPR: evidence and fallacy. *J Control Release* 2014;190:451-464.
23. Cheng L, Yang T, Zhang J, Gao F, Yang L, Tao W. The application of radiolabeled targeted molecular probes for the diagnosis and treatment of prostate cancer. *Korean J Radiol* 2023;24:574-589.